JOURNAL OF Materials CHEMISTRY

Photoluminescent organic–inorganic composite films layer-by-layer self-assembled from the rare-earth-containing polyoxometalate $Na_9[EuW_{10}O_{36}]$ and poly(allylamine hydrochloride)

Yonghui Wang,[a] Xinlong Wang,[a] Changwen Hu*[a] and Chunshan Shi[b]

[a]*Institute of Polyoxometalate Chemistry, Faculty of Chemistry, Northeast Normal University, Changchun 130024, P. R. China. E-mail: huchw@nenu.edu.cn*
[b]*Changchun Institute of Applied Chemistry, Academia Sinica, Changchun, Jilin 130022, P. R. China*

Received 26th July 2001, Accepted 13th November 2001
First published as an Advance Article on the web 29th January 2002

Photoluminescent organic–inorganic composite films incorporating the rare-earth-containing polyoxometalate $Na_9[EuW_{10}O_{36}]$ (EW) and poly(allylamine hydrochloride) (PAH) have been prepared by the layer-by-layer self-assembly method. UV-vis spectroscopy and ellipsometry were used to follow the fabrication process of the EW/PAH composite films. The experimental results show that the deposition process is linear and highly reproducible from layer to layer. An average EW/PAH bilayer thickness of *ca.* 2.1 nm was determined by ellipsometry. In addition, scanning electron microscopy and atomic force microscopy images of the EW/PAH composite films indicate that the film surface is relatively uniform and smooth. The photoluminescent properties of these films were investigated by fluorescence spectroscopy.

1 Introduction

Organic–inorganic hybrid or composite materials are currently the subject of intense interest in the field of materials science, as they can exhibit synergetic electrical, magnetic and optical properties.[1] In particular, organic–inorganic composite films assembled from nanoscale building blocks with various organic and inorganic compositions possess potential applications in many areas, including microelectronics, non-linear optics, and electroluminescent devices.[2–6] Several techniques, such as Langmuir–Blodgett (LB) deposition,[7–10] sol–gel processing,[11,12] and layer-by-layer (LbL) self-assembly[13–24] have been employed to produce these composite films. The layer-by-layer (LbL) self-assembly method, originally developed by Decher and co-workers to prepare multilayer assemblies of organic polymers,[25–28] has provided a simple, yet powerful, approach for the fabrication of a variety of ordered organic–inorganic composite films that incorporate organic polyelectrolytes and inorganic materials such as graphite oxide,[13–15] clay,[16–18] zirconium phosphate,[19] and nanoparticles.[20–23] This technique, based on the sequential adsorption of oppositely charged species from dilute solutions, is particularly attractive, since it permits assembly of different organic and inorganic building blocks into well-defined ultrathin composite films with controlled thickness and controlled molecular architecture at the nanometer level on essentially arbitrary solid substrates.[3,28] In addition, compared with the LB deposition technique, this method is advantageous in the low cost of instrumentation and high throughput of layer fabrication.[22]

Polyoxometalates (POMs) constitute a significant class of inorganic compounds and are attracting much attention as building blocks for functional composite materials because of their particularly interesting nanosized structures[29,30] and their potential applications in catalysis, conductivity, photo- and electrochromic devices and molecular electronics.[31,32] However, practical applications of POMs in these areas rely largely on the successful fabrication of thin POM-containing films.[33] Several reports have shown that the LbL method is also adaptable for the preparation of ultrathin organic–inorganic composite films from a cationic polyelectrolyte and a negatively charged POM.[33–36] However, these reports focus mainly on the assembly process and adsorption mechanism of the composite films, while the properties of these films as materials are rarely reported.[34] In addition, to our knowledge, no reports on the fabrication of organic–inorganic composite films incorporating rare-earth-containing POMs by the LbL method have been published up till now.

Here, we present the first fabrication of ultrathin organic–inorganic composite films of a rare-earth-containing POM, $Na_9[EuW_{10}O_{36}]$ (EW), and poly(allylamine hydrochloride) (PAH) by the layer-by-layer self-assembly method. The composite films are characterized by UV-vis spectroscopy, ellipsometry, scanning electron microscopy (SEM), and atomic force microscopy (AFM). The photoluminescent properties of these films have been investigated by fluorescence spectroscopy.

2 Experimental

Poly(sodium 4-styrenesulfonate) (PSS), MW 70 000, and poly(allylamine hydrochloride) (PAH), MW 70 000, were purchased from Tokyo Chemical Industry Co., Ltd. Poly(ethyleneimine) (PEI), MW 50 000, was obtained from Aldrich. All polyelectrolytes were used without further purification. The rare-earth-containing polyoxometalate EW was prepared as described by Peacock and Weakley (see ref. 37) with the composition $Na_9[EuW_{10}O_{36}]\cdot\sim 18H_2O$. Sodium chloride (AR grade) was obtained commercially and used as received. The deionized water used for all experiments and for all cleaning steps was passed through an Elgastat UHQ purification system. The resistivity was about 18 $M\Omega\,cm^{-1}$.

All solid substrates (quartz or single crystal silicon) were cleaned with "piranha solution', a 30 : 70 mixture of 30% hydrogen peroxide (H_2O_2) and concentrated sulfuric acid (H_2SO_4) at 80 °C for 1 h, and thoroughly rinsed with deionized water. Further purification was carried out by immersion in a solution containing NH_4OH (29 wt% aqueous solution), H_2O_2

(30 wt% aqueous solution), and pure water with a volume ratio 1 : 1 : 5 at 70 °C for 20 min and then extensively washing with water. The cleaned substrates were dried with nitrogen prior to use.

The following solutions were used to prepare EW/PAH organic–inorganic composite films: 10^{-2} M PEI in water, 10^{-2} M PSS in 1 M NaCl, 10^{-2} M PAH in 1 M NaCl (pH ~ 5–6), and 10^{-3} M EW in water (pH ~ 5–6). The polyelectrolyte concentration was based on the molecular weight of the monomer unit. The fabrication of EW/PAH LbL composite films was carried out by first depositing a PEI/PSS/PAH precursor film (P) onto a cleaned substrate with an immersion time of 20 min for each adsorption, followed by rinsing with deionized water and drying in nitrogen after each immersion. After this procedure, the uppermost layer on the substrate was PAH, which provides a positively-charged surface for subsequent self-assembly of an EW layer. The substrate was then dipped into the EW solution for 20 min, followed by immersion in the PAH solution for 20 min, rinsing with deionized water for 1 min and drying in a nitrogen stream after each dipping. This procedure resulted in the buildup of an EW/PAH bilayer and can be repeated until the desired number of bilayers is built up. All adsorption procedures were performed at room temperature. The composite architecture thus obtained can be expressed as P/(EW/PAH)$_n$.

The composite films were characterized by the following methods. UV-vis absorption spectra were recorded on a 756 CRT UV-vis spectrophotometer (Shanghai, China). Ellipsometric data were acquired by using an AUEL-III automated laser ellipsometer (Xi'an Jiaotong University, China) with a 2 mW HeNe laser (λ = 632.8 nm) light source and an angle of incidence of 70° for silicon substrates. Thickness data are average values from different spots (5–6) on a given sample. Scanning electron micrographs were obtained on a Hitachi S-570 scanning electron microscope operating at 20 kV. Atomic force micrographs were taken using a Digital Nanoscope IIIa instrument operating in the noncontact mode with pyramidal tips and cantilevers made from etched silicon probes. Photoluminescence spectra were obtained at room temperature with a SPEX FL-2T2 fluorescence spectrophotometer with double gratings.

3 Results and discussion

UV-vis spectroscopy has proved to be a useful and facile technique to evaluate the growth process of multilayers[33–36] and was thus used in the present work to monitor the LbL assembly process of EW/PAH organic–inorganic composite films. Fig. 1 shows the UV-vis absorption spectra of (EW/PAH)$_n$ multilayers (with n = 7) assembled on a precursor PEI/PSS/PAH film on quartz substrates. The inset in Fig. 1 presents the plots of the absorbance values for these multilayer films at 195 and 260 nm as a function of the number of deposition cycles. As shown in Fig. 1, these films exhibit the characteristic bands of EW at 195 and 260 nm corresponding to the oxygen → tungsten charge transfer (CT) transitions,[38] substantiating the incorporation of EW polyanions into the composite film without any alteration. The feature at 225 nm for the precursor film is due to the benzene chromophores in PSS,[33,36] while PAH does not absorb above 200 nm.[33] Since the f → f bands of Eu^{3+} in the visible region are very weak and can only be seen by using concentrated solutions,[37] the UV-vis spectra of the EW/PAH composite films do not show these bands. As shown in the inset of Fig. 1, the absorbances of quartz-supported P/(EW/PAH)$_n$ multilayer composite films at two characteristic wavelengths (195 and 260 nm) increase proportionally with the number of deposition cycles, n. This nearly linear growth of the absorption peaks indicates that an approximately equal amount of EW is deposited for each

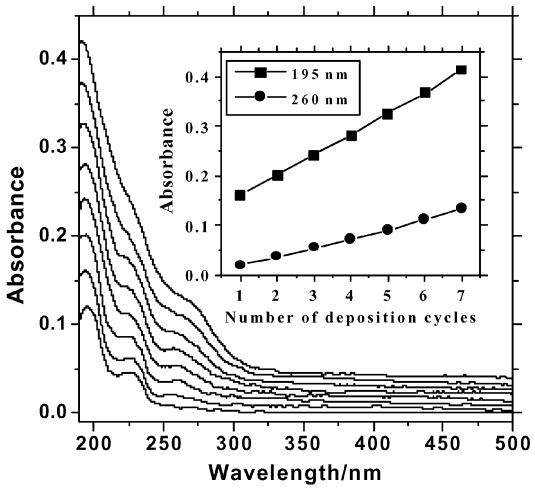

Fig. 1 UV-vis absorption spectra of (EW/PAH)$_n$ multilayer films with n = 0–7 on PEI/PSS/PAH-modified quartz substrates. The lowest curve corresponds to the precursor film (n = 0). The other curves, from bottom to top, correspond to n = 1, 2, 3, 4, 5, 6, and 7, respectively. The inset shows plots of the absorbance values at 195 and 260 nm as a function of the number of deposition cycles (n).

adsorption procedure and that the EW/PAH composite films grow uniformly with each deposition cycle. Furthermore, the average values of the absorbance increment for each additionally adsorbed EW/PAH bilayer are calculated to be *ca.* 0.045 at 195 nm and 0.018 at 260 nm, respectively. Given the fact that PAH contributes no absorption in this wavelength range,[33] these absorbances are due to EW only. (These values are for films assembled on both sides of the quartz substrates.) In addition, one may notice that extrapolation of linear regression curves toward n = 0 for the absorbance values at 195 and 260 nm do not pass through the origin. This indicates the greater amount of EW adsorbed by the PEI/PSS/PAH precursor film and may be explained by the penetration of the EW polyanions into the underlying precursor film.[33]

According to the literature, the surface concentration, Γ, of EW on the PAH surface in each EW/PAH bilayer can be calculated using $\Gamma = [(A_\lambda/2)\varepsilon_\lambda{}^{-1}N_A] \times 10^{-3}$, where A_λ is the absorbance of EW in one EW/PAH bilayer at a given wavelength (λ), ε_λ is the extinction coefficient of EW in solution (M^{-1} cm^{-1}) at λ, and N_A is Avogadro's number.[33,39] Based on the absorbance values in the wavelength range of 190–280 nm and the corresponding molar extinction coefficients calculated from the absorption spectrum of the aqueous EW solution, the average surface concentration of EW per bilayer is calculated to be *ca.* 2.92×10^{14} clusters cm^{-2} or 4.85×10^{-10} mol cm^{-2} for (EW/PAH)$_n$ multilayer films. These values are comparable with those obtained by Fendler *et al.* for ultrathin films of poly(diallyldimethylammonium chloride) and sodium decatungstate self-assembled on quartz (6.2×10^{-10} mol cm^{-2}) and on mica (4.9×10^{-10} mol cm^{-2}),[34] but is about sixteen times that for the molybdenum polyoxometalate (Mo_{57})–polyelectrolyte multilayer films prepared by Caruso *et al* [$(1.4 \pm 0.4) \times 10^{13}$ clusters cm^{-2}].[33] We assume that this difference originates from many factors, including the processing and type of the substrate, the concentration of the solution, the nature of the polyanion, and the adsorption time. In our case, the strongly hydrophilic nature of the substrate after processing and the high concentration of the EW solution (10^{-3} M, five times that of the Mo_{57} solution used by Caruso *et al.*[33]) are perhaps responsible for the much greater surface concentration, as the concentrations of the polyelectrolytes and the adsorption time employed are the same in both cases.

The uniform multilayer growth of EW/PAH organic–inorganic assemblies is also confirmed by optical ellipsometry measurements. The thickness of the multilayered structure

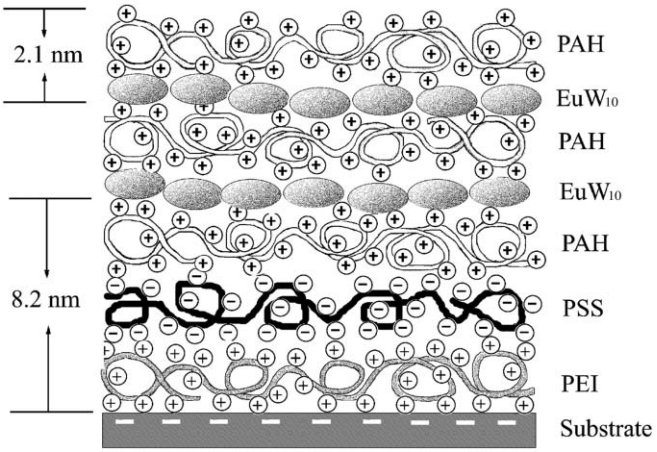

Fig. 2 Schematic representation of the internal layer structure of a PEI/PSS/PAH/(EW/PAH)$_3$ multilayer film self-assembled on a substrate. Note that this drawing is an oversimplification of the actual layer structure.

increases linearly with the number of deposition cycles. This clearly demonstrates that in each adsorption cycle equivalent amounts of EW and PAH are deposited on the substrates and that deposition is very reproducible and film growth is essentially uniform. From ellipsometry the average film thickness for the EW/PAH bilayer is determined to be *ca.* 2.1 nm. In view of the 1.2 nm film thickness for a single PAH layer,[36,40] the remaining 0.9 nm can thus be assigned to the EW layer. This value is consistent with the cluster diameter of EW in the short axis (*ca.* 0.8 nm).[41] Therefore, the EW polyanions may be oriented in the EW/PAH bilayer with their short axis normal to the surface of the substrate and form a monolayer (see Fig. 2). In addition, ellipsometric measurements also establish a thickness of $\sim$8.2 nm for the precursor PEI/PSS/PAH film.

In order to obtain some detailed information about the surface morphology and the homogeneity of the EW/PAH organic–inorganic composite films prepared by LbL self-assembly, scanning electron microscopy and atomic force microscopy investigations were performed. Fig. 3 shows a SEM image of a P/(EW/PAH)$_{10}$ multilayer film prepared on a silicon wafer. It is obvious that the film surface is relatively smooth over a large area. However, this SEM image also shows some

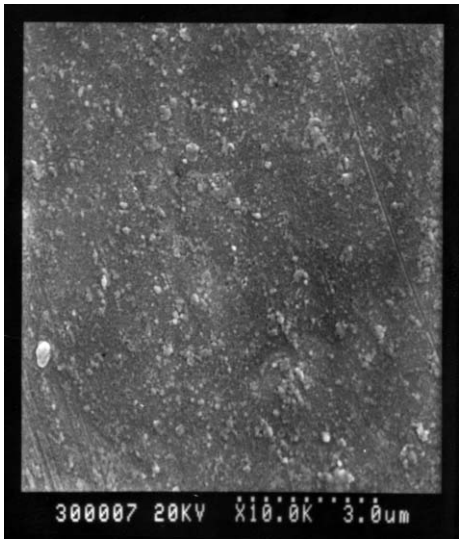

Fig. 3 Scanning electron micrograph of a P/(EW/PAH)$_{10}$ multilayer on a silicon wafer (surface view).

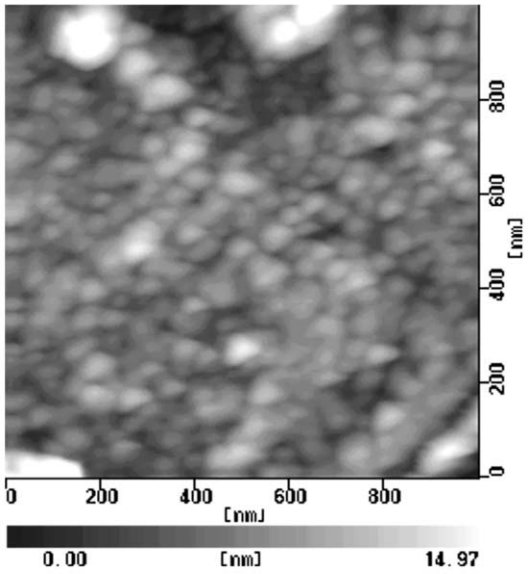

Fig. 4 AFM image of a P/(EW/PAH)$_n$ multilayer on a silicon wafer (n = 3).

individual domains which are perhaps bi- and multilayer aggregates of the EW polyanions and/or the PAH polyelectrolyte chains.[34]

The topography of silicon-supported (EW/PAH)$_n$ films was also investigated by AFM in the noncontact mode, which provided insight into the internal structure of the multilayers. Fig. 4 displays an AFM image of the surface of a P/(EW/PAH)$_3$ organic–inorganic composite film. In general, the composite film is relatively uniform and smooth. However, in fact, it is made up of a large number of small domains with diameters of *ca.* 60–80 nm along the horizontal axis. These domains are probably composed of complex ion pairs formed by the association of the EW polyanions with PAH polyelectrolyte chains *via* electrostatic interactions. The roughness of the film surface was estimated to be about 3.0 nm.

Fig. 5(a) shows the photoluminescence spectrum of a solid sample of EW and Fig. 5(b) shows those of P/(EW/PAH)$_n$ composite films (n = 1, 8, and 15) self-assembled on a smooth quartz substrate and excited at room temperature. The inset in Fig. 5(b) indicates the increases in the intensities of some emission bands of the composite films with the number of deposition cycles. When $[EuW_{10}O_{36}]^{9-}$ is excited in the intense UV bands corresponding to the oxygen–tungsten transitions within the $[EuW_{10}O_{36}]^{9-}$ ''ligand', or in the weak bands corresponding to f–f excited states of the Eu^{3+} ion in the visible region, at room temperature, weak luminescence arising from the $^5D_0 \rightarrow {}^7F_J$ (J = 0, 1, 2, 3, 4) transitions can be observed.[38,42,43] As shown in Fig. 5, for the EW/PAH film, the photoluminescence spectrum exhibits multiple peak structure, very similar to that found for the EW solid. This again confirms that the structure of $[EuW_{10}O_{36}]^{9-}$ is retained after incorporation into the film, that is, the $[EuW_{10}O_{36}]^{9-}$ polyanions can exist in the film stably. As can be seen, the most intense bands at *ca.* 590 and 595 nm correspond to the $^5D_0 \rightarrow {}^7F_1$ emission transition. The broad band around 621 nm is also relatively intense and is ascribed to the $^5D_0 \rightarrow {}^7F_2$ emission transition. The less intense bands at 693 and 701 nm are assigned to the $^5D_0 \rightarrow {}^7F_4$ emission transition, while the very small band at *ca.* 652 nm corresponds to the $^5D_0 \rightarrow {}^7F_3$ emission transition.[38,42,43] However, for both the EW solid and the EW/PAH composite films, the $^5D_0 \rightarrow {}^7F_0$ emission transition cannot be observed, since it is forbidden in nature[38,43] and is commonly observed in complexes with some asymmetry, this fact is not surprising and thus suggests a symmetric

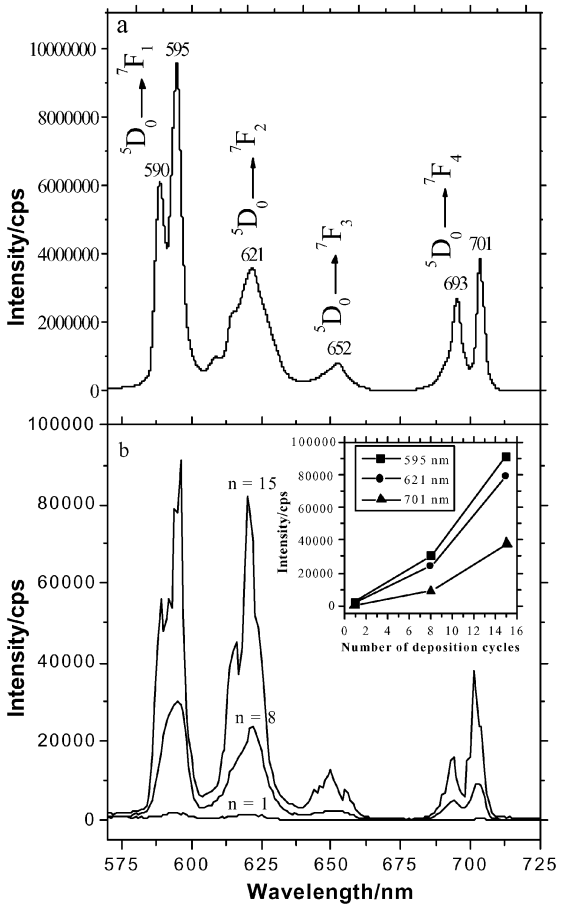

Fig. 5 Photoluminescence spectra of a solid sample of EW (a) and P/(EW/PAH)$_n$ multilayer films (n = 1, 8 and 15) assembled on a quartz substrate (b), both excited in the UV region at room temperature. The inset in (b) indicates the increases in the intensities of some emission bands (595, 621, and 701 nm) of the composite films with the number of deposition cycles.

environment about the Eu^{3+} ion in the EW polyanion for both solid and composite films. This is also supported by the relatively low intensity of the $^5D_0 \rightarrow {}^7F_2$ band. In addition, for Fig. 5(a) and (b), there are some differences in the relative intensity, multiplicity, and width of individual bands. This may arise from the fact that the content of EW is relatively low and that the symmetry and distribution of EW in the film are different from those in the solid. Furthermore, one can see from the inset in Fig. 5(b) that the relative intensity of the emission for the composite films increases with the number of deposition cycles. This result also confirms the high reproducibility of film fabrication by the layer-by-layer self-assembly method.

4 Conclusions

In this paper we have demonstrated a simple but powerful strategy based on layer-by-layer self-assembly for the preparation of ultrathin organic–inorganic composite films that incorporate the rare-earth-containing polyoxometalate $Na_9[EuW_{10}O_{36}]$ and the polyelectrolyte poly(allylamine hydrochloride). The films display a linear increase in the absorption and film thickness with the number of deposition cycles. SEM and AFM images indicate that the films are relatively uniform and smooth. The photoluminescent properties of the multilayer composite films are similar to those observed for the EW solid, which is of potential importance to the fabrication of photoluminescent thin film materials incorporating POMs. This method may be adaptable to other POMs and studies in this respect are currently underway.

Acknowledgement

The present work was supported by the National Natural Science Foundation of China (20071007) and the Foundation for University Key Teachers of the Chinese Ministry of Education.

References

1 C. R. Kagan, D. B. Mitzi and C. D. Dimitrakopoulos, *Science*, 1999, **286**, 945.
2 V. L. Colvin, M. C. Schlamp and A. P. Alivisatos, *Nature*, 1994, **370**, 354.
3 T. Cassagneau, T. E. Mallouk and J. H. Fendler, *J. Am. Chem. Soc.*, 1998, **120**, 7848.
4 M. Gao, B. Richter, S. Kirstein and H. Möhwald, *J. Phys. Chem. B*, 1998, **102**, 4096.
5 D. M. Kaschak and T. E. Mallouk, *J. Am. Chem. Soc.*, 1996, **118**, 4222.
6 J. H. Fendler and F. C. Meldrum, *Adv. Mater.*, 1995, **7**, 607.
7 K. B. Blodgett and I. Langmuir, *Phys. Rev.*, 1937, **51**, 964.
8 Y. Tian and J. H. Fendler, *Chem. Mater.*, 1996, **8**, 969.
9 I. Moriguchi, H. Maeda, Y. Teraoka and S. Kagawa, *J. Am. Chem. Soc.*, 1995, **117**, 1139.
10 Y. Tian, C. Wu and J. H. Fendler, *J. Phys. Chem.*, 1995, **99**, 3736.
11 I. Ichinose, H. Senzu and T. Kunitake, *Chem. Lett.*, 1996, 831.
12 I. Moriguchi, H. Maeda, Y. Teraoka and S. Kagawa, *Chem. Mater.*, 1997, **9**, 1050.
13 N. A. Kotov, I. Dékány and J. H. Fendler, *Adv. Mater.*, 1996, **8**, 637.
14 T. Cassagneau and J. H. Fendler, *Adv. Mater.*, 1998, **10**, 877.
15 N. I. Kovtyukhova, P. J. Ollivier, B. R. Martin, T. E. Mallouk, S. A. Chizhik, E. V. Buzanevz and A. D. Gorchinskiy, *Chem. Mater.*, 1999, **11**, 771.
16 E. R. Kleinfeld and G. S. Ferguson, *Science*, 1994, **265**, 370.
17 N. A. Kotov, T. Haraszti, L. Turi, G. Zavala, R. E. Geer, I. Dékány and J. H. Fendler, *J. Am. Chem. Soc.*, 1997, **119**, 6821.
18 N. A. Kotov, S. Magonov and E. Tropsha, *Chem. Mater.*, 1998, **10**, 886.
19 S. W. Keller, H. N. Kim and T. E. Mallouk, *J. Am. Chem. Soc.*, 1994, **116**, 8817.
20 N. A. Kotov, I. Dékány and J. H. Fendler, *J. Phys. Chem.*, 1995, **99**, 13065.
21 Y. Liu, A. Wang and R. Claus, *J. Phys. Chem. B*, 1997, **101**, 1385.
22 J. Schmitt, G. Decher, R. E. Geer, R. Shashidhar and J. M. Calvert, *Adv. Mater.*, 1997, **9**, 61.
23 E. Hao and T. Lian, *Langmuir*, 2000, **16**, 7879.
24 T. Sasaki, Y. Ebina, M. Watanabe and G. Decher, *Chem. Commun.*, 2000, 2163.
25 G. Decher and J. D. Hong, *Makromol. Chem., Makromol. Symp.*, 1991, **46**, 321.
26 G. Decher, J. D. Hong and J. Schmitt, *Thin Solid Films*, 1992, **210/211**, 831.
27 Y. Lvov, F. Essler and G. Decher, *J. Phys. Chem.*, 1993, **97**, 13773.
28 G. Decher, *Science*, 1997, **277**, 1232.
29 S. Zhang, G. Huang, M. Shao and Y. Tang, *J. Chem. Soc., Chem. Commun.*, 1993, 37.
30 A. Müller, E. Krickemeyer, S. Dillinger, H. Bögge, W. Plass, A. Proust, L. Dloczik, C. Menke, J. Meyer and R. Z. Rohlfing, *Anorg. Allg. Chem.*, 1994, **620**, 599.
31 For a recent overview on polyoxometalate chemistry, refer to: C. L. Hill, *Chem. Rev.*, 1998, **98**, and references therein.
32 Y. Guo, Y. Wang, C. Hu, Y. Wang and E. Wang, *Chem. Mater.*, 2000, **12**, 3501.
33 F. Caruso, D. G. Kurth, D. Volkmer, M. J. Koop and A. Müller, *Langmuir*, 1998, **14**, 3462.
34 I. Moriguchi and J. H. Fendler, *Chem. Mater.*, 1998, **10**, 2205.
35 I. Ichinose, H. Tagawa, S. Mizuki, Y. Lvov and T. Kunitake, *Langmuir*, 1998, **14**, 187.
36 D. G. Kurth, D. Volkmer, M. Ruttorf, B. Richter and A. Müller, *Chem. Mater.*, 2000, **12**, 2829.
37 R. D. Peacock and T. J. R. Weakley, *J. Chem. Soc. A*, 1971, 1836.
38 R. Ballardini, Q. G. Mulazzani, M. Venturi, F. Bolletta and V. Balzani, *Inorg. Chem.*, 1984, **23**, 300.

39 D. Li, B. I. Swanson, J. M. Robinson and M. A. Hoffbauer, *J. Am. Chem. Soc.*, 1993, **115**, 6975.
40 G. Decher, in *Comprehensive Supramolecular Chemistry*, ed. J. L. Atwood, J. E. D. Davies, D. D. MacNicol and F. Vögtle, Pergamon, Oxford, 1996, vol. 9, p. 507.
41 M. Sugeta and T. Yamase, *Bull. Chem. Soc. Jpn.*, 1993, **66**, 444.
42 M. J. Stillman and A. J. Thomson, *J. Chem. Soc., Dalton Trans.*, 1976, 1138.
43 G. Blasse, G. J. Dirksen and F. J. Zonnevijlle, *J. Inorg. Nucl. Chem.*, 1981, **43**, 2847.